$(Sr,Mn)TiO_3$—a magnetoelectrically coupled multiglass

2008 J. Phys.: Condens. Matter 20 434216

(http://iopscience.iop.org/0953-8984/20/43/434216)

J. Phys.: Condens. Matter **20** (2008) 434216 (6pp) doi:10.1088/0953-8984/20/43/434216

(Sr, Mn)TiO_3—a magnetoelectrically coupled multiglass

W Kleemann[1,3], V V Shvartsman[1], S Bedanta[1], P Borisov[1], A Tkach[2] and P M Vilarinho[2]

[1] Angewandte Physik, Universität Duisburg-Essen, Lotharstraße 1, 47048 Duisburg, Germany
[2] Department of Ceramics and Glass Engineering, CICECO, University of Aveiro, 3810-193, Aveiro, Portugal

E-mail: wolfgang.kleemann@uni-due.de

Received 20 March 2008
Published 9 October 2008
Online at stacks.iop.org/JPhysCM/20/434216

Abstract

Extending the framework for multiferroic materials, in which long-range electric and magnetic orderings coexist, we present a novel 'multiglass' concept, where two different glassy states occur simultaneously. It applies to $Sr_{0.98}Mn_{0.02}TiO_3$ ceramics, where the Mn^{2+} dopant ions are at the origin of both polar and spin glasses. Spin freezing is initiated at the dipolar glass temperature, $T_g \approx 38$ K. Below T_g, both glass phases are independently verified by memory and rejuvenation effects. Strong biquadratic interaction of the Mn^{2+} spins with the optic soft mode of the incipient ferroelectric host crystal $SrTiO_3$ explains the high spin glass temperature and comparably strong higher order magnetoelectric coupling between the polar and magnetic degrees of freedom.

(Some figures in this article are in colour only in the electronic version)

1. Introduction

During the last few years the intensity of studies on multiferroic—e.g. simultaneously ferromagnetic and ferroelectric—materials [1, 2] has strongly increased. This is partly due to the high potential for applications of the magnetoelectric (ME) effect [3] expected in this class of compounds [4, 5]. The variations of magnetic properties on applying electric fields and the converse effect promise to open attractive possibilities for producing novel kinds of sensors, memory devices and driving elements [6–8].

In this paper we show that the class of ME materials may be extended to those undergoing transitions into glassy states. These are well known to occur as a result of competing interactions and topological frustration, where the glass transition temperature T_g separates the ergodic high temperature regime, $T > T_g$, from the non-ergodic low T one. At $T < T_g$ true thermodynamic equilibrium is reached only asymptotically. Structural and spin glass states at low T are established by cooperative random freezing of the dipolar [9] and of the spin degrees of freedom, respectively [10]. Here we report on the simultaneous existence of a magnetic spin glass and a polar glass state as well as on their mutual ME coupling in $SrTiO_3$ moderately doped with Mn^{2+} (SMnT, for short).

[3] Author to whom any correspondence should be addressed.

2. Doped incipient ferroelectrics

$SrTiO_3$ belongs to the family of incipient ferroelectrics, where the polar instability at the transition into the ferroelectric state is suppressed by quantum fluctuations and the system remains in the non-polar paraelectric state down to 0 K [11]. Polar properties in STO can be induced by various ionic substitutions as in $(Sr_{1-x}Ca_x)TiO_3$ [12] or in $SrTi(^{16}O_{1-x}{}^{18}O_x)_3$ [13]. In the related solid solution SMnT with $x \leqslant 0.03$, slim polarization ($\boldsymbol{P}$) versus electric field ($\boldsymbol{E}$) hysteresis loops and a broad strongly frequency dependent peak of the temperature dependence of the dielectric permittivity, $\varepsilon(T)$, are found [14–16]. The polar state in these compounds has been shown by ESR techniques [17] to be due to off-center shifts of the Mn^{2+} cations at the twelvefold-coordinated A cation (referring to Sr^{2+}) positions within the perovskite structure as shown in figure 1(a). The off-center Mn^{2+} cations are assumed to create dipoles, which induce polar clusters in the highly polarizable $SrTiO_3$ host lattice [18, 19]. Their size corresponds to the polarization correlation length, ξ [20]. Hence, the

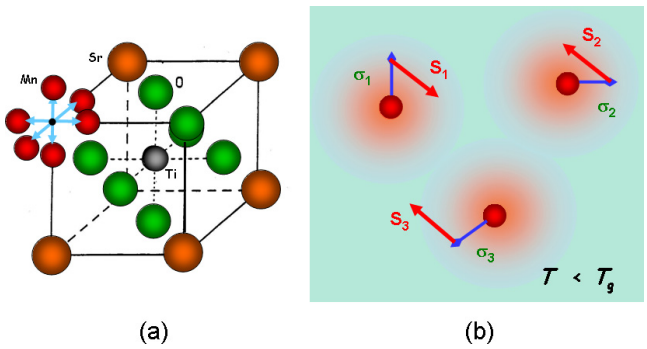

Figure 1. (a) Displacement vectors of an off-center Mn^{2+} ion in A site doped $SrTiO_3$. (b) Frustrated arrangement of three antiferromagnetically interacting Mn^{2+} spins, S_j, $j = 1, 2$ and 3, occupying frozen off-center positions σ_j of the structural glass backbone at temperatures below T_g.

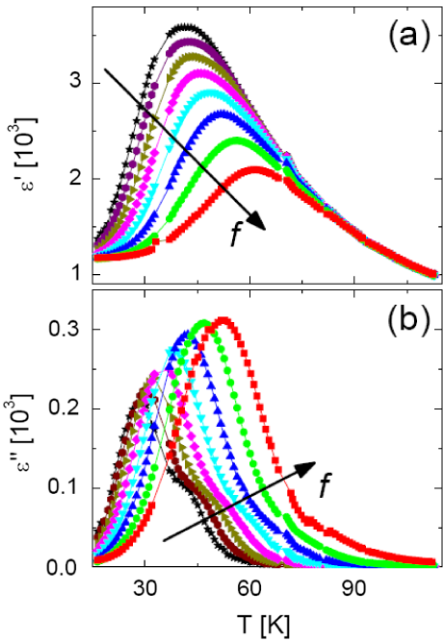

Figure 2. Temperature dependences of the real and imaginary parts, ε' (a) and ε'' (b), respectively, of the dielectric permittivity of a $Sr_{0.98}Mn_{0.02}TiO_3$ ceramic recorded at frequencies $f = 100$ mHz, 1 Hz, 10 Hz, 100 Hz, 1 kHz, 10 kHz, 100 kHz and 0.4 MHz as indicated by arrows.

situation resembles that for the related (non-magnetic!) system $(K_{1-x}Li_x)TaO_3$ (KLT) [6], which undergoes glassy freezing at $T_g < 40$ K for $x < 0.022$ [21]. Mean-field theory and Monte Carlo simulations [22] have shown that the dipolar and structural ('quadrupolar') degrees of freedom in KLT are, indeed, able to undergo transitions into generic glass states. In the case of figure 1(a) a six-state Potts glass is supposed to occur.

3. Dielectric properties of Mn doped $SrTiO_3$

Ceramic samples of SMnT with $x = 0.02$ were prepared by a mixed oxide technology described elsewhere [15]. Preponderant incorporation of Mn^{2+} into A sites of the perovskite structure was confirmed by energy dispersive x-ray spectra [16] and by Mn^{2+} ESR analysis [17]. Lowering the previously chosen frequency range [19] by three orders of magnitude, figure 2 shows the temperature dependence of the complex dielectric permittivity $\varepsilon = \varepsilon' - i\varepsilon''$ recorded at frequencies $10^{-1} \leqslant f < 10^6$ Hz. The emerging broad and strongly frequency dependent peaks of both components, $\varepsilon'(T)$ (a) and $\varepsilon''(T)$ (b), are related to the dynamics of polar clusters created by off-center displacements of Mn^{2+} cations [19]. The position of the peak temperature T_m of $\varepsilon'(T)$ is well described by a power law of the respective frequency, $f(T_m) \propto (T_m/T_g - 1)^{z\nu}$ [23], which is a typical manifestation of glassy critical behavior [24]. Best fits of our experimental data yield the glass temperature $T_g = 38.3 \pm 0.3$ K and the dynamical critical exponent, $z\nu = 8.5 \pm 0.2$, which compares well with that of spin glass systems [24]. Obviously at T_g the dynamics of the polar clusters becomes frozen, where the relaxation time $\tau = (2\pi f)^{-1}$ diverges on a percolating network, thus defining a phase transition from the disordered superparaelectric to a cluster glass state. Similarities with superspin glass characteristics [24] are obvious. We shall see below that this freezing process initiates also the transition of the Mn^{2+} spin moments into a spin glass state.

Another strong indicator of the suspected structural glass state is the memory effect, which arises after isothermally annealing the sample below T_g. Figure 3(a) shows an example of the resulting 'hole burning' in $\varepsilon'(T)$ after a wait time $t_w \approx 10.5$ h at the waiting temperature $T_w = 32.5$ K. We find a negative peak at T_w, $\varepsilon'_{wait}(T_w) - \varepsilon'_{ref}(T_w) \approx -6$. The relative decrease, $\Delta\varepsilon'/\varepsilon' \approx -0.002$, is very small, but definitely beyond errors, and resembles that observed for the structural glass $KTa_{0.973}Nb_{0.027}O_3$ [25]. It signifies the asymptotic approach to the glassy ground state at T_w, via a decrease of susceptibility with respect to an external homogeneous field ('stiffening'). Since the structure of the glassy ground state varies as a function of the temperature, the system is 'rejuvenating' at temperatures sufficiently far from T_w [24]. Hence, the 'burnt hole' is strongly localized around T_w. This contrasts with the global decrease expected for an ordinarily relaxing metastable system. The small value of the memorized 'hole' seems to indicate that only a small fraction of the total system is actually freezing. Indeed, it should be noticed that the structural glassy freezing of SMnT does not signify a complete immobilization of all hopping Mn^{2+} ions around their A sites (figure 1(a)). It rather means that just one percolating cluster freezes and achieves the global relaxation time $\lim_{f\to 0}\tau = \infty$, while ramifications and clusters of smaller size are still able to relax at finite frequencies. This may be judged from ε'' versus $\log f$ spectra as shown previously [23]. Since ε'' measures the distribution function of relaxation times, its extension over more than nine decades of frequencies clearly signifies the glassy nature of the system. At low frequencies, $f < 10^{-1}$ Hz, the low f branch of $\varepsilon''(T)$ is observed to gradually lift up and to become horizontal at $T < 38.9$ K. Thus it virtually extends to $f_{min} \to 0$ with finite amplitude, similar to what is observed for the relaxation spectra of $K_{0.989}Li_{0.011}TaO_3$ [18] and of spin glassy manganese aluminosilicate [26].

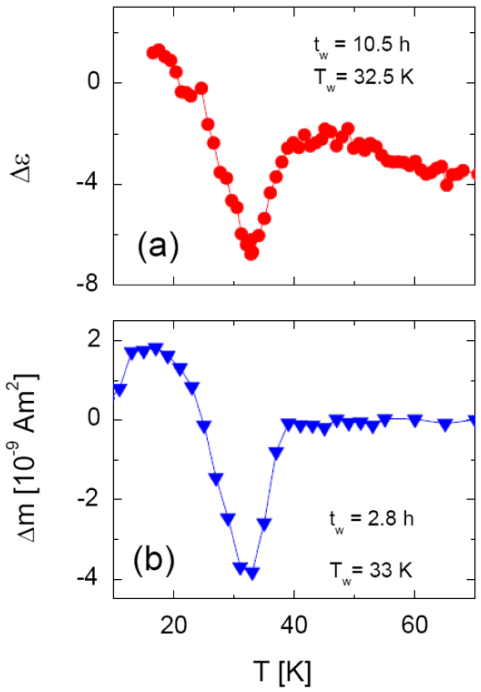

Figure 3. (a) Difference curve $\Delta\varepsilon' = \varepsilon'_{\rm wait} - \varepsilon'_{\rm ref}$ versus T obtained at $f = 10$ Hz and $E_{\rm ac} = 60$ V m^{-1} upon heating after zero-field cooling from 80 K and waiting for 10.5 h at $T_{\rm w} = 32.5$ K ('$\varepsilon'_{\rm wait}$') or without waiting ('$\varepsilon'_{\rm ref}$'). (b) Difference curve of $m^{\rm ZFC-FH}$ with and without intermittent stops of $t_{\rm w} = 2.8$ h at $T_{\rm w} = 33$ K and measured in $\mu_0 H = 10$ mT after ZFC from 110 to 5 K.

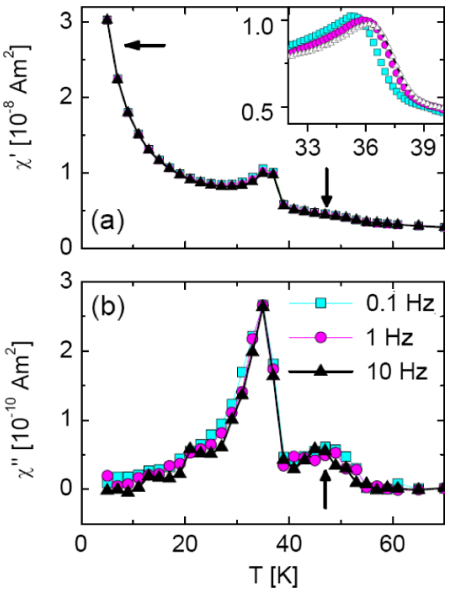

Figure 4. Temperature dependence within $5 \leqslant T \leqslant 70$ K of the real and the imaginary parts, χ' (a) and χ'' (b), of the magnetic ac susceptibility of $Sr_{0.98}Mn_{0.02}TiO_3$ ceramics measured at frequencies $10^{-1} \leqslant f \leqslant 10$ Hz with a field amplitude $\mu_0 H_{\rm ac} = 0.4$ mT. The inset in (a) shows the weak frequency dispersion of χ' in an expanded view. Vertical arrows denote anomalies related to peaks in $\varepsilon(T)$ as shown in figure 2. The horizontal arrow in (a) denotes the Curie-type signal of 'free' magnetic moments.

4. Magnetic properties of Mn doped $SrTiO_3$

Figure 4 shows the temperature dependence of the real and imaginary components of the magnetic ac susceptibility, χ' (a) and χ'' (b), respectively, measured with an amplitude of $\mu_0 H = 0.4$ mT at frequencies $0.1 \leqslant f \leqslant 10$ Hz. Pronounced peaks are observed in both quantities slightly below $T_{\rm g} \approx 38$ K. Compared to the strongly polydispersive dielectric permittivity spectra (figures 2(a) and (b)) the frequency dispersion of the magnetic susceptibility is rather weak and becomes sizable only below $T_{\rm g}$ (figure 4(a), inset). Furthermore, the relatively high temperature of the magnetic anomaly is surprising. For comparison, other insulators like manganese aluminosilicate show spin glass peaks of the susceptibility at a doping level as high as 16.3% only below 4 K [27]. Obviously in SMnT at a Mn^{2+} concentration of merely 2%, a decisive amplification effect needs to be considered. In analogy to the antiferromagnetic quantum paraelectric $EuTiO_3$ [28] we assume strong coupling of spin and structural pseudospin components expressed by a biquadratic coupling Hamiltonian,

$$H^{\rm me} = -\delta \sum_{\langle i,j \rangle} \sum_{\langle k,l \rangle} S_i S_j \sigma_k \sigma_l, \qquad (1)$$

describing both the observed large spin–phonon coupling [29] and sizable magnetocapacitive effects [26]. The pseudospin components $\sigma_{k,l}$ mimic both the off-center displacements of the A site dopant ions (Mn^{2+}) and the displacements of the B site Ti^{4+} ions, which participate in the optic soft mode. δ is an effective coupling constant. The displacement correlation functions couple to the $S = 5/2$ Heisenberg spins $S_{i,j}$ of the $3d^5$ configuration of the Mn^{2+} ions. Large effects are expected around $T_{\rm g}$, where the structural pair correlation functions $\langle \sigma_k \sigma_l \rangle$ maximize, promote increased spin pair correlation functions $\langle S_i S_j \rangle$ and thus give rise to the anomalies of the magnetic susceptibility (figures 4(a) and (b)).

Below $T_{\rm g}$, the onset of a percolating structural network of the frozen polar clusters probably triggers the freezing of the spin degrees of freedom into a spin glass state. This is understood as follows. Above $T_{\rm g} \approx 38$ K the Mn^{2+} spins are subjected to the hopping motion of the Mn^{2+} ions. They have, hence, no chance to acquire a stable spin glass ground state, which is very sensitive to quenched structural disorder. This explains the lack of dispersion of the magnetic susceptibility above $T_{\rm g}$, where the superparaelectric structural dynamics suppresses any glassy spin clustering. Only at $T \leqslant T_{\rm g}$ do those spins residing on the percolating glass cluster have a chance to freeze into a well-defined ground state. Its nature will be glassy, since antiferromagnetic superexchange interaction between the Mn^{2+} spins via Mn–O–Mn chains can be supposed in the oxidic environment of $SrTiO_3$ rather than a ferromagnetic one. The situation resembles the frustrated interaction scheme of dilute manganese aluminosilicate spin glasses [27]. A sketch of a possible frustrated local spin configuration at three sites of the frozen structural cluster is depicted in figure 1(b). It should be stressed that the average distance between Mn^{2+} ions in SMnT with $x = 0.02$, $\langle d \rangle \approx 1.5$ nm, is too large for stability of the spin glass structure to be achieved solely through frustrated superexchange [27].

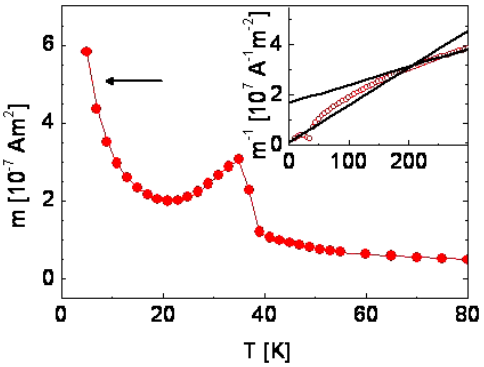

Figure 5. Temperature dependence of $m^{\mathrm{ZFC-FH}}$ measured in a magnetic field of $\mu_0 H = 10$ mT. The low T Curie-type behavior is indicated by a horizontal arrow. The inset shows $1/m^{\mathrm{ZFC-FH}}$ within $5 \leqslant T \leqslant 300$ K, where the asymptotic high and low T slopes are indicated by solid lines.

The interaction, equation (1), is a decisive additional ingredient which promotes glassy ordering of the spin subsystem via the structural glassy order below T_g.

Two further anomalies of the magnetic susceptibility merit mentioning. On one hand the low temperature response is asymptotically of the Curie type, $\chi' \propto 1/T$ (figure 4(a), horizontal arrow), while $\chi'' \cong 0$ (figure 4(b)). This indicates that a sizable fraction of uncoupled spins remain paramagnetic down to lowest temperatures. In order to estimate the remaining fraction of paramagnetic ions we approximate the zero-field cooling–low field ($\mu_0 H = 10$ mT) heating (ZFC–FH) magnetization curve in figure 5 by the Curie law

$$m^{\mathrm{ZFC-FH}} = (N m_0^2 / 3 k_B T) \mu_0 H, \qquad (2)$$

both at high and low temperatures, where N is the respective number of paramagnetic ions, m_0 their individual magnetic moment and k_B Boltzmann's constant. An 'atomic' moment $m_0 \approx 5\ \mu_B$, coming close to the literature value $m(\mathrm{Mn}^{2+}) = 5.92\ \mu_B$ [31], emerges from the total number of Mn^{2+} ions, $N \approx 1.3 \times 10^{19}$, as calculated from the sample mass, and the Curie constant at high temperatures, $T > 250$ K. A plot of $1/m^{\mathrm{ZFC-FH}}$ in the inset to figure 5 clearly distinguishes a flat slope between 250 and 300 K from a steeper one below about 30 K. This manifests the process of condensation of the ions into the spin glass phase. From equation (2) we can estimate that about 60–70% of the Mn^{2+} ions remain paramagnetic at low T, a certain fraction of which occupy ill-defined interfacial positions of the ceramic sample. The remaining 30–40% belong to the spin glass state. This is consistent with the idea that only those spins which reside on the rare percolating structural glass cluster are subject to glassy freezing, and underlines the intimate relationship between frozen dipoles and frozen spins. They occupy the same subsystem of lattice sites (figure 1(b)) and are subject to coupling between local polar and magnetic order parameters.

On the other hand, weak dispersion steps of χ' (a) and peaks of χ'' (b) are observed in figure 4 between 40 and 55 K (vertical arrows), where also peaks of ε' and ε'' are encountered (figures 2(a) and (b)). This is another manifestation of the coupling of electric and magnetic dipolar degrees of freedom.

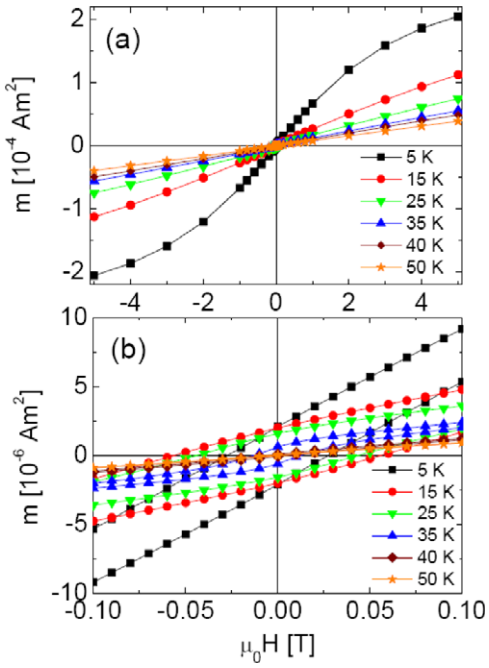

Figure 6. (a) Magnetic moment, m, versus applied magnetic field, $\mu_0 H$, measured within $-5 \leqslant \mu_0 H \leqslant 5$ T at different temperatures in the interval $5 \leqslant T \leqslant 50$ K for a $Sr_{0.98}Mn_{0.02}TiO_3$ ceramic. The solid lines are guides to the eye. (b) Zoomed view of the above hysteresis loops measured within $-0.1 \leqslant \mu_0 H \leqslant 0.1$ T.

In order to confirm that the previously observed anomalies of magnetization and hysteresis below 40 K [23] are generic properties of a spin glass phase, we have looked for a memory effect similar to that for the structural glass freezing (figure 3(a)). Figure 3(b) shows the differences between $m^{\mathrm{ZFC-FH}}$ data recorded with and without an intermittent stop, $\Delta m^{\mathrm{ZFC}}(T) = m^{\mathrm{ZFC}}_{\mathrm{wait}}(T) - m^{\mathrm{ZFC}}_{\mathrm{ref}}(T)$, obtained after a wait time of $t_w = 2.8$ h at the wait temperature T_w ($<T_g$) = 33 K. Indeed, a sharply defined dip due to 'hole burning' occurs exactly at T_w like in figure 3(a). Its absence at $T_w > T_g$ has been ascertained (not shown). The observed 'hole burning' clearly evidences rejuvenation of the spin system outside the immediate vicinity of T_w, as reported for atomic and superspin glasses [24].

Curves of magnetization m versus $\mu_0 H$ (figures 6(a) and (b)) reveal finite remanence and coercivity in hysteresis loops below 40 K. These are due to field-induced metastable states of the spin glass phase. Actually, as remarked above, the $m(\mu_0 H)$ curves in figures 6(a) and (b) contain two contributions: one from individual paramagnetic Mn^{2+} ions and another one related to the spin glass state below T_g (see above). The two contributions are not expected to saturate at the fields available, $|\mu_0 H| \leqslant 5$ T, and are not easily distinguishable [10].

5. Magnetoelectric coupling

The proposed biquadratic coupling, equation (1), has spherical symmetry and is valid under all symmetry point groups including C_1. Hence, it does not require any special crystal

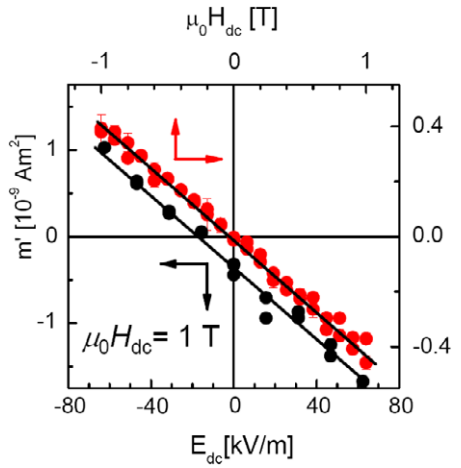

Figure 7. Real part m' of the ac susceptibility measured at $T = 10$ K and $f = 1$ Hz in an ac electric field with amplitude $E_{ac} = 62.5$ kV m^{-1} versus H_{dc} ($-1 \leqslant \mu_0 H_{dc} \leqslant 1$ T; upper loop) and versus E_{dc} ($-62.5 \leqslant E_{dc} \leqslant 62.5$ kV m^{-1}) under a bias field $\mu_0 H_{dc} = 1$ T (lower loop).

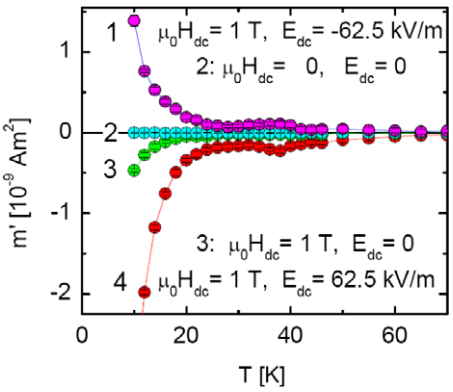

Figure 8. Real part m' versus T of the ac susceptibility due to an ac electric field with amplitude $E_{ac} = 62.5$ kV m^{-1} measured at $f = 1$ Hz under bias fields $\mu_0 H_{dc} = 0$ or 1 T and $E_{dc} = 0$ or ± 62.5 kV m^{-1} as indicated (curves 1–4) in the temperature interval $10 \leqslant T \leqslant 70$ K.

or spin structure [32]. Intuitively, within a Landau free energy density expansion [33] it is supposed to be the first non-vanishing coupling parameter for glassy materials. Further possible ME coupling terms up to the biquadratic contribution might nevertheless be tested for their existence. They read for SMnT as follows, disregarding spontaneous polarization, spontaneous magnetization and linear ME coupling in the absence of an appropriate crystalline symmetry [34]:

$$F(\mathbf{E},\mathbf{H}) = F_0 - \tfrac{1}{2}\varepsilon_0\varepsilon_{ij}E_iE_j - \tfrac{1}{2}\mu_0\mu_{ij}H_iH_j - \frac{\beta_{ijk}}{2}E_iH_jH_k - \frac{\gamma_{ijk}}{2}H_iE_jE_k - \frac{\delta_{ijkl}}{2}E_iE_jH_kH_l \quad (3)$$

under Einstein summation. The electric field-induced components of the magnetization

$$\mu_0 M_i = -\partial F/\partial H_i = \mu_0\mu_{ij}H_j + \frac{\gamma_{ijk}}{2}E_jE_k + \beta_{ijk}E_jH_k + \delta_{ijkl}H_jE_kE_l \quad (4)$$

are readily measured using modified SQUID susceptometry [35]. This involves ac and dc electric and magnetic external fields, $E = E_{ac}\cos\omega t + E_{dc}$ and H_{dc}, and records the first-harmonic complex ac magnetic moment, $m'(t) = (m' - \mathrm{i}m'')\cos\omega t$, where

$$m' = (\beta E_{ac}H_{dc} + \gamma E_{ac}E_{dc} + 2\delta E_{ac}E_{dc}H_{dc})(V/\mu_0) \quad (5)$$

(V = sample volume). At the measurement frequency $f = \omega/2\pi = 1$ Hz the imaginary part, m'', has proven negligible. In order to obtain the orientation averaged coupling constants β, γ and δ we performed three experiments after cooling the sample in zero external field to $T = 10$ K.

First, we tested the quadratic ME response, $m' \propto \gamma E^2$, with $E_{ac} = 62.5$ kV m^{-1}, $E_{dc} = \pm 62.5$ kV m^{-1} and $H_{dc} = 0$. The signals obtained lie within the noise level, $m' = (2 \pm 7)$ and $(0.8 \pm 8) \times 10^{-12}$ A m^2; hence, $\gamma \approx 0$.

Second, we applied $E_{ac} = 62.5$ kV m^{-1} and $E_{dc} = 0$, and cycled the magnetic field, $|\mu_0 H_{dc}| \leqslant 1$ T (figure 7, upper curve). The slope of the emerging linear hysteresis-free cycle yields $\beta = -\mu_0\Delta m'/VE_{ac}H_{dc} \approx -3.0 \times 10^{-19}$ s A^{-1}. Surprisingly, despite the low concentration of 'ferro-active' Mn^{2+} ions, $|\beta|$ is larger than that for the concentrated crystalline low T antiferromagnet $BaMnF_4$, $\beta_{xxx} = 1.1 \times 10^{-19}$ s A^{-1} [36]. Such 'giant' coupling strength is obviously due to the above mentioned dipolar clustering in the quantum paraelectric $SrTiO_3$ host lattice. The observed EH^2 term of the free energy and the corresponding electric field dependent '*paramagnetoelectric*' susceptibility, $\Delta m'/\Delta H_{dc} \propto E_{ac}$, are allowed whenever the paramagnetic ions are located at sites with broken inversion symmetry [37] and do not require magnetic long-range order [38] in accordance with our structure model depicted for low T (figure 1(b)). It is beyond the scope of this paper to explain the observed negative sign of β, which requires extensive crystal field calculations [37].

Third, we applied $E_{ac} = 62.5$ kV m^{-1} and $\mu_0 H_{dc} = 1$ T, and cycled an electric field, $|E_{dc}| \leqslant 62.5$ kV m^{-1} (figure 7, lower curve). This cycle is, again, linear and non-hysteretic. According to equation (5) it reveals βEH and δHE^2 from the intercept at $E_{dc} = 0$ and from the slope of m' versus E_{dc}, respectively. Consistently, the same β value emerges as from the slope of the upper curve, $\beta = -3.0 \times 10^{-19}$ s A^{-1}, while the biquadratic coefficient—measured for the first time to the best of our knowledge—is $\delta = -\mu_0\Delta m'/(2VH_{dc}E_{ac}\Delta E_{dc}) \approx -9.0 \times 10^{-24}$ sm V^{-1} A^{-1}. The negative sign of δ seems to support double glassiness. The value of δ allows us to predict the magnetocapacitive effect with $(\Delta\varepsilon)_{E^2H^2} = \delta H^2/\varepsilon_0 \approx -0.65$ (using equation (3) and inserting $\mu_0 H = 1$ T) and $\varepsilon'(T = 10\ \mathrm{K},\ f = 1\ \mathrm{Hz}) \approx 1300$ (figure 2(a)); hence, $\Delta\varepsilon/\varepsilon' \approx -5 \times 10^{-4}$. Its magnitude is about 2.5% of that found for crystalline $EuTiO_3$ at $\mu_0 H = 1$ T and $T = 4$ K, $\Delta\varepsilon/\varepsilon' = \alpha < S_iS_j \gtrsim 2 \times 10^{-2}$ [30], in accordance with the low concentration of the Mn^{2+} ions in SMnT.

Further insight into the interdependence of the magnetoelectric responses and the linear magnetic susceptibility is provided by m' versus T measured on heating from $T = 10$ K (figure 8). Different constant fields, E_{dc} and $\mu_0 H_{dc}$, were applied. While $E_{dc} = 0 = \mu_0 H_{dc}$ yields $m' \equiv 0$ as expected in the absence of the linear ME effect, a moderate magnetic

field, $\mu_0 H_{dc} = 1$ T, generates a small ME moment via the EH^2 effect, $m'(10\,\mathrm{K}) = -5 \times 10^{-10}$ A m^2, which vanishes as $T \to T_g$.

Much larger ME moments, $|m'| \leqslant 3 \times 10^{-9}$ A m^2, are found under the simultaneous action of two dc fields, $E_{dc} = \pm 62.5$ kV m^{-1} and $\mu_0 H_{dc} = 1$ T. In agreement with the lower curve in figure 7, the magnitude of m' increases by about a factor of two upon changing the sign of E_{dc} due to the superimposed EH^2 effect. In close resemblance with the case for the susceptibility, χ' versus T (figure 4(a)), the H^2E^2 effects maximize at low temperatures, decrease rapidly on heating, but peak again at $T_g = 38$ K, $|m'| \approx 2 \times 10^{-10}$ A m^2. Being roughly proportional to $\chi'\langle\sigma_i\sigma_j\rangle$, the low T increase is certainly due to that of the paramagnetic susceptibility, while the peak at T_g is related to that of the dipolar correlation function $\langle\sigma_i\sigma_j\rangle$. Remarkably, the H^2E^2 effect fades out on heating only far above T_g at $T \approx 70$ K. This confirms its compatibility with all symmetries, including C_1 for the paraelectric one. We notice that the weak out-of-phase signal, m'' (not shown), is about one order of magnitude smaller than $|m'|$, nearly vanishes under EH^2, but peaks under H^2E^2 conditions at both T_g and $T \to 0$.

6. Conclusion

Quantum paraelectric strontium titanate has, again, delivered novel and surprising features. When replacing diamagnetic Sr^{2+} ions by a small amount of magnetic Mn^{2+} ions, two different processes are activated at low temperatures. On one hand, the Mn^{2+} ions take the role of electric and elastic pseudospins as is known, e.g., from the orientational glass (K, Li)TaO_3, and undergo a transition into a structural six-state Potts glass [22]. On the other hand, the $S = 5/2$ spins, being attached to the rattling (at high T) and frozen (at low T) Mn^{2+} ions, couple via frustrated antiferromagnetic superexchange, reinforced by magnetoelectric two-spin–pseudospin interaction. They freeze into a spin glass state as soon as the structural degrees of freedom come to rest on a percolating dipolar glass backbone below $T_g = 38$ K. Both glassy phases are unambiguously and independently evidenced by their specific ageing and memory effects. Dipolar and magnetic 'holes' have never before been burnt into one and the same system. Comparable strength of the magnetoelectric coupling via the '*magnetocapacitive*' H^2E^2 and via the '*paramagnetoelectric*' EH^2 effects manifests the importance of dipolar clustering due to quantum fluctuations in $SrTiO_3$. It will be interesting to repeat these experiments on oriented (Sr, Mn)TiO_3 single crystals in order to verify the symmetry of the different ME coupling schemes in detail. This is, however, still a challenge for crystal growers, who up to now have not succeeded in performing exclusively A site substitution [39].

Acknowledgments

Financial support by the European Community within STREP NMP3-CT-2006-032616 (MULTICERAL), by the European Network of Excellence FAME under contract FP6-500159-1, by the Deutsche Forschungsgemeinschaft via KL306/38-3 and Sonderforschungsbereich 491, and by the DAAD via Acções Integradas Luso-Alemãs is gratefully acknowledged.

References

[1] Hur N, Park S, Sharma P A, Ahn J S, Guha S and Cheong S-W 2004 *Nature* **429** 392
[2] Fiebig M, Lottermoser T, Goltsev A V and Pisarev R V 2002 *Nature* **419** 818
[3] Fiebig M 2005 *J. Phys. D: Appl. Phys.* **38** R123
[4] Brown W F, Hornreich R M and Shtrikman S 1968 *Phys. Rev.* **168** 574
[5] Eerenstein W, Mathur N D and Scott J F 2006 *Nature* **442** 759
[6] Wang N, Cheng J, Pyatakov A, Zvezdin A K, Li J F, Cross L E and Viehland D 2005 *Phys. Rev.* B **72** 104434
[7] Lottermoser T and Fiebig M 2004 *Phys. Rev.* B **70** 220407(R)
[8] Goto T, Kimura T, Lawes G, Ramirez A P and Tokura Y 2004 *Phys. Rev. Lett.* **92** 257201
[9] Höchli U T, Knorr K and Loidl A 1990 *Adv. Phys.* **39** 405
[10] Binder K and Young A P 1986 *Rev. Mod. Phys.* **58** 801
[11] Müller K A and Burkard H 1979 *Phys. Rev.* B **19** 3593
[12] Bednorz J G and Müller K A 1984 *Phys. Rev. Lett.* **52** 2289
[13] Itoh M, Wang R, Inamura Y, Yamaguchi T, Shan Y-J and Nakamura T 1999 *Phys. Rev. Lett.* **82** 3540
[14] Tkach A, Vilarinho P M and Kholkin A L 2005 *Appl. Phys. Lett.* **86** 172902
[15] Tkach A, Vilarinho P M and Kholkin A L 2005 *Acta Mater.* **53** 5061
[16] Tkach A, Vilarinho P M and Kholkin A L 2006 *Acta Mater.* **54** 5385
[17] Laguta V V *et al* 2007 *Phys. Rev.* B **76** 054104
[18] Bianchi U, Dec J, Kleemann W and Bednorz J G 1995 *Phys. Rev.* B **51** 8737
[19] Tkach A, Vilarinho P M and Kholkin A L 2007 *J. Appl. Phys.* **101** 084110
[20] Vugmeister B and Glinchuk M D 1990 *Rev. Mod. Phys.* **62** 993
[21] Wickenhöfer F, Kleemann W and Rytz D 1991 *Ferroelectrics* **124** 237
[22] Vollmayr H, Kree R and Zippelius A 1991 *Phys. Rev.* B **44** 12238
[23] Shvartsman V V, Bedanta S, Borisov P, Kleemann W, Tkach A and Vilarinho P M 2008 *Phys. Rev. Lett.* submitted
[24] Jönsson P E 2004 *Adv. Chem. Phys.* **128** 191
[25] Doussineau P, de Lacerda-Aroso T and Levelut A 1999 *Europhys. Lett.* **46** 401
[26] Wenger L E 1983 *Lecture Notes in Physics* vol 192 (Berlin: Springer) p 60
[27] Huang F S *et al* 1978 *J. Phys. C: Solid State Phys.* **11** L271
[28] Gong S J and Jiang Q 2004 *Phys. Status Solidi* b **241** 3033
[29] Fennie C J and Rabe K M 2006 *Phys. Rev. Lett.* **96** 205505
[30] Katsufuji T and Takagi H 2001 *Phys. Rev.* B **64** 054415
[31] Kittel Ch 1966 *Introduction to Solid State Physics* 3rd edn (New York: Wiley) p 509
[32] Fennie C J and Rabe K 2006 *Phys. Rev. Lett.* **97** 267602
[33] Rivera J-P 1994 *Ferroelectrics* **161** 165
[34] Landau L D and Lifshitz E M 1960 *Electrodynamics of Continuous Media* (Oxford: Pergamon) p 119
[35] Borisov P, Hochstrat A, Shvartsman V V and Kleemann W 2007 *Rev. Sci. Instrum.* **78** 106105
[36] Sciau Ph, Clin M, Rivera J-P and Schmid H 1990 *Ferroelectrics* **105** 201
[37] Hou S L and Bloembergen N 1965 *Phys. Rev.* **138** A1218
[38] Schmid H 1994 *Ferroelectrics* **161** 1
[39] Badalyan A K *et al* 2007 *11th European Mtg on Ferroelectricity (Bled, Slovenia, Sept. 2007)* p 70 (Book of Abstracts)